

# Density functional calculations of diffusion paths of $\text{CH}_3\text{S}_{\text{ad}}$ on $c(2\times 2)\text{-Cl}$ and $\text{-Br}$ covered $\text{Cu}(100)$ surfaces

## Supporting Information

F. Wendorff<sup>(1)</sup> and E. Pehlke<sup>(1,2)</sup>

<sup>(1)</sup> Institut für Theoretische Physik und Astrophysik  
Christian-Albrechts-Universität zu Kiel  
Olshausenstr. 40, 24098 Kiel, Germany

<sup>(2)</sup> Kiel Nano, Surface and Interface Science KiNSIS, Kiel University,  
Germany

## Contents

|          |  |           |
|----------|--|-----------|
| <b>1</b> | <b>Convergence Analysis</b>  | <b>2</b>  |
| 1.1      | Number of Cu layers . . . . .  | 3         |
| 1.2      | Cut-off Energy . . . . .   | 4         |
| 1.3      | Vacuum width . . . . .   | 5         |
| 1.4      | $\mathbf{k}$ -point grid . . . . .   | 6         |
| 1.5      | Threshold for residual force orthogonal to the diffusion path . . . . .  | 7         |
| <b>2</b> | <b><math>\text{CH}_3\text{S}_{\text{ad}}</math> diffusion on <math>\text{Cu}(100)</math> without halogen co-adsorbates</b>   | <b>8</b>  |
| <b>3</b> | <b>Comparison of rotation path of <math>\text{S}_{\text{ad}}</math> with Rahn et al.</b>   | <b>10</b> |
| <b>4</b> | <b>Diffusion paths for <math>\text{S}_{\text{ad}}</math> and <math>\text{CH}_3\text{S}_{\text{ad}}</math> on a halogen covered <math>\text{Cu}(100)</math> surface</b> | <b>12</b> |
|          | <b>Acknowledgments</b>   | <b>21</b> |
|          | <b>References</b>  | <b>22</b> |

# 1 Convergence Analysis

To determine the accuracy of the density functional calculations, a convergence analysis has been carried through. We have tested the convergence with respect to the cut-off energy of the plane-wave expansion of the wavefunctions, the density of the  $\mathbf{k}$ -point mesh, the thickness of the Cu slab, the vacuum thickness, and, for the NEB calculations, the maximum residual force that is allowed to act orthogonally to the NEB path. In order to estimate the accuracy of the calculations with respect to each of these parameters, the energy difference for Cl<sub>ad</sub>, Br<sub>ad</sub> and S<sub>ad</sub> at the bridge and the hollow site of the Cu(100) substrate surface has been calculated within a p(2×2) cell. The total error for the calculations is taken as the sum of the errors for the individual parameters. For each parameter always the largest error among the three different adsorbates has been considered. The total error for total energy differences is estimated as

$$\Delta E_{\text{tot}} = \Delta E_{\text{layers}} + \Delta E_{\text{cutoff}} + \Delta E_{\text{vacuum}} + \Delta E_{\text{kpoints}} + \Delta E_{\text{path}} \quad (1)$$

and the total error regarding variations of the dipole moment along diffusion reaction paths is

$$\Delta \mu_{\text{tot}} = \Delta \mu_{\text{layers}} + \Delta \mu_{\text{cutoff}} + \Delta \mu_{\text{vacuum}} + \Delta \mu_{\text{kpoints}} . \quad (2)$$

Note that this estimate does not include the inaccuracy due to our choice of the approximate XC-energy functional. It is assumed to be much larger than the convergence error. All calculations reported in this paper have been carried through for adsorbates on a Cu(100) surface in vacuum.

Unless otherwise specified the convergence tests have been carried out using a p(2×2) cell with six copper layers, where the bottom two copper layers are fixed at their bulk positions (bulk lattice constant equal to 3.637 Å) and the top four Cu layers are relaxed. The cut-off energy of the plane-waves basis set has been set to 35 Ry. A grid of 12×12×1  $\mathbf{k}$ -points are evenly distributed over the first Brillouin zone in reciprocal space according to Monkhorst and Pack [20] and the vacuum width between the asymmetric slabs is 16 Å with a dipole correction midway. The pseudopotentials used in the calculations are listed in Table S1.

Table S1: Pseudopotentials used in the DFT calculations.

| Element | Potential file                 | Ref. |
|---------|--------------------------------|------|
| H       | H.pbe-rrkjus.UPF               | [3]  |
| C       | c_pbe_v1.2.uspp.F.UPF          | [6]  |
| S       | s_pbe_v1.4.uspp.F.UPF          | [9]  |
| Cl      | cl_pbe_v1.4.uspp.F.UPF         | [8]  |
| Cu      | Cu.pbe-dn-rrkjus_psl.1.0.0.UPF | [5]  |
| Br      | br_pbe_v1.4.uspp.F.UPF         | [7]  |

## 1.1 Number of Cu layers

Figure S1 shows the energy difference and Figure S2 shows the difference in the dipole moment from the hollow to the bridge position for the adsorbates  $\text{Cl}_{\text{ad}}$ ,  $\text{Br}_{\text{ad}}$  and  $\text{S}_{\text{ad}}$  on a Cu(100) surface in a  $p(2 \times 2)$  cell for a number of Cu-layers between six and 18 with the bottom two layers fixed at the bulk positions. From this follows for a calculation with six copper layers an error of  $\Delta E_{\text{layers}} = 10 \text{ meV}$  and  $\Delta \mu_{\text{layers}} = 2 \text{ me}\text{\AA}$ .

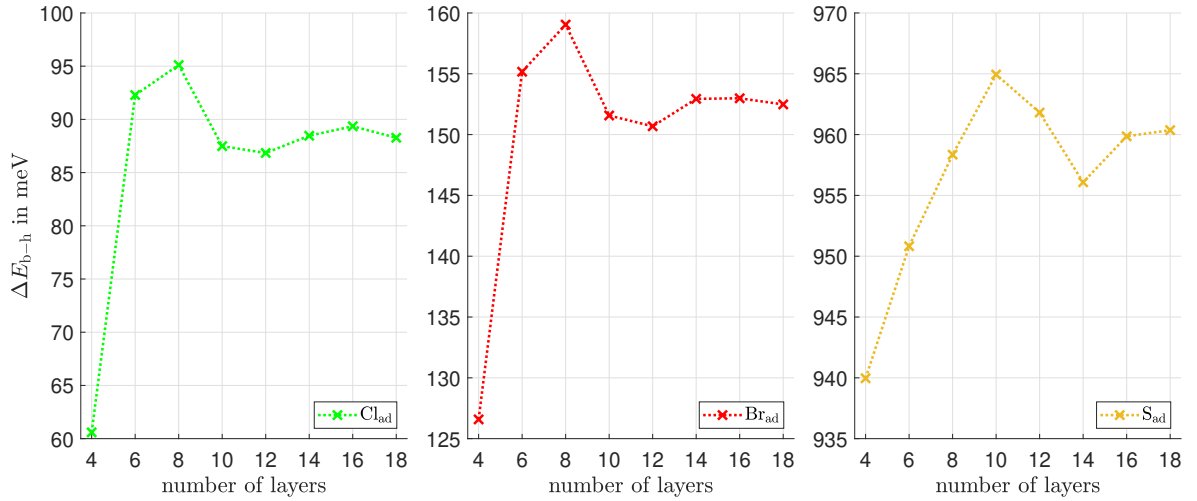


Figure S1: Difference of the energy of  $\text{Cl}_{\text{ad}}$ ,  $\text{Br}_{\text{ad}}$  and  $\text{S}_{\text{ad}}$  between hollow and bridge position as a function of the number of copper layers.

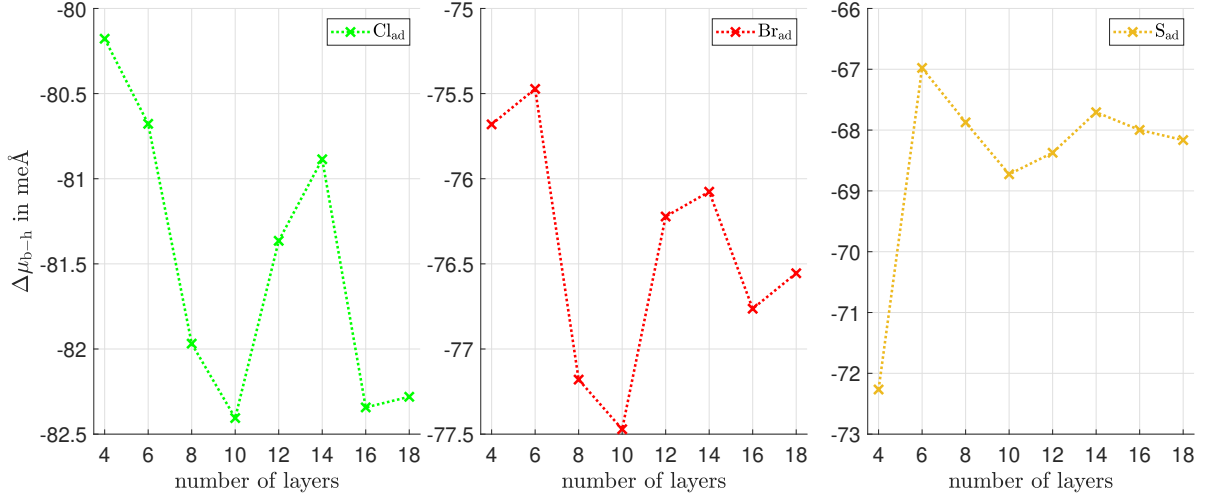


Figure S2: Difference of the dipole moment of Cl<sub>ad</sub>, Br<sub>ad</sub> and S<sub>ad</sub> between hollow and bridge position as a function of the number of copper layers.

## 1.2 Cut-off Energy

Figure S3 shows the energy difference and Figure S4 shows the difference in the dipole moment from the hollow to the bridge position for the adsorbates Cl<sub>ad</sub>, Br<sub>ad</sub> and S<sub>ad</sub> on a Cu(100) surface in a p(2×2) cell for a cut-off energy for the wavefunctions between 25 Ry and 79 Ry. From this follows for a calculation with a cut-off of 35 Ry (476 eV) an error of  $\Delta E_{\text{cutoff}} = 1$  meV and  $\Delta\mu_{\text{cutoff}} = 0.5$  meÅ.

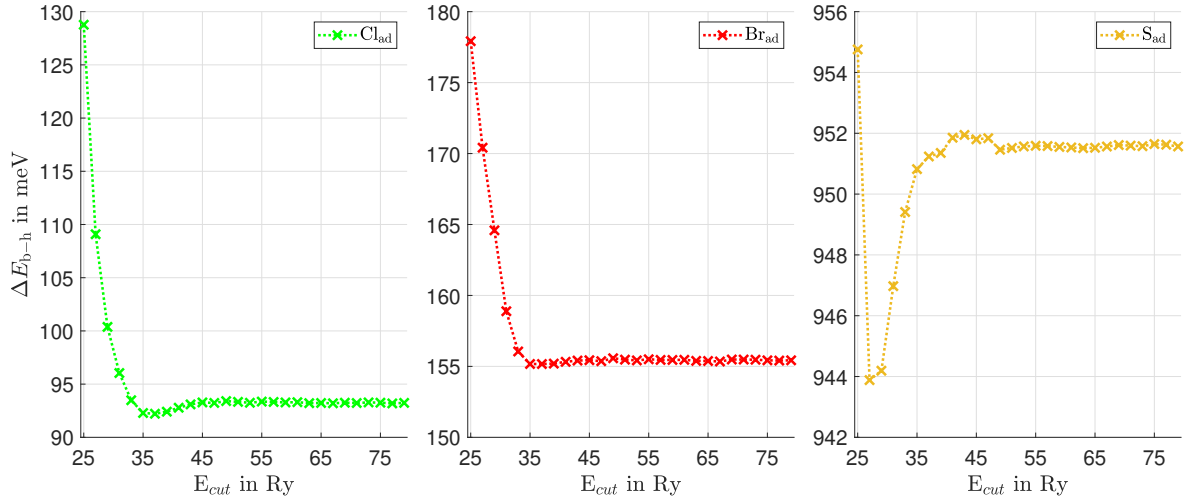


Figure S3: Difference of the energy of Cl<sub>ad</sub>, Br<sub>ad</sub> and S<sub>ad</sub> between hollow and bridge position as a function of the cut-off energy for the wavefunctions.

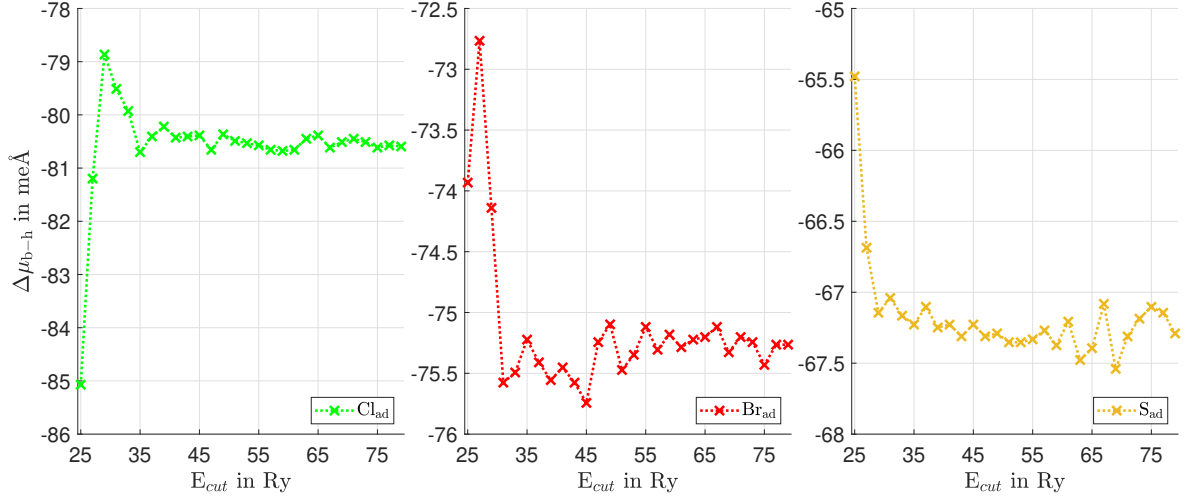


Figure S4: Difference of the dipole moment of  $\text{Cl}_{\text{ad}}$ ,  $\text{Br}_{\text{ad}}$  and  $\text{S}_{\text{ad}}$  between hollow and bridge position as a function of the cut-off energy for the wavefunctions.

### 1.3 Vacuum width

Figure S5 shows the energy difference and Figure S6 shows the difference in the dipole moment from the hollow to the bridge position for the adsorbates  $\text{Cl}_{\text{ad}}$ ,  $\text{Br}_{\text{ad}}$  and  $\text{S}_{\text{ad}}$  on a  $\text{Cu}(100)$  surface in a  $p(2 \times 2)$  cell for a vacuum width between  $7 \text{ \AA}$  and  $25 \text{ \AA}$  with a dipole correction in the middle of the vacuum. From this follows for a calculation with a vacuum of  $16 \text{ \AA}$  an error of  $\Delta E_{\text{vacuum}} < 1 \text{ meV}$  and  $\Delta \mu_{\text{vacuum}} = 0.3 \text{ meÅ}$ .

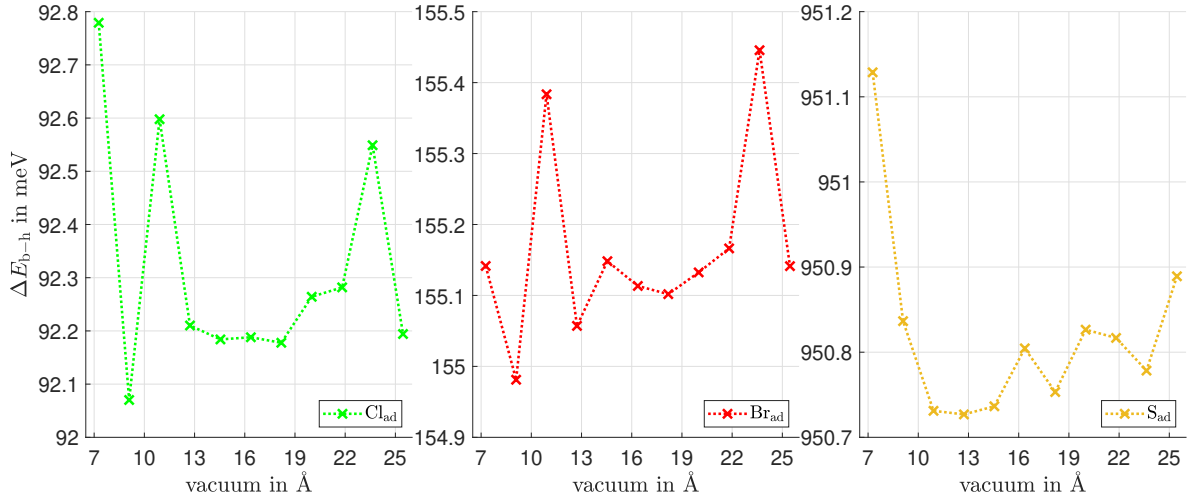


Figure S5: Difference of the energy of  $\text{Cl}_{\text{ad}}$ ,  $\text{Br}_{\text{ad}}$  and  $\text{S}_{\text{ad}}$  between hollow and bridge position as a function of the width of the vacuum between the slabs.

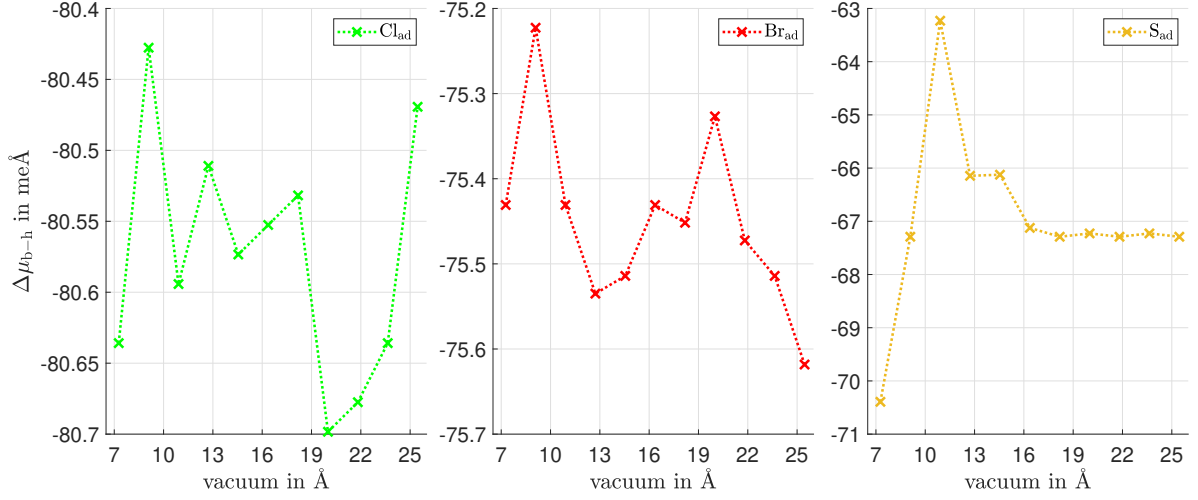


Figure S6: Difference of the dipole moment of  $\text{Cl}_{\text{ad}}$ ,  $\text{Br}_{\text{ad}}$  and  $\text{S}_{\text{ad}}$  between hollow and bridge position as a function of the width of the vacuum between the slabs.

## 1.4 k-point grid

Figure S7 shows the energy difference and Figure S8 shows the difference in the dipole moment from the hollow to the bridge position for the adsorbates  $\text{Cl}_{\text{ad}}$ ,  $\text{Br}_{\text{ad}}$  and  $\text{S}_{\text{ad}}$  on a Cu(100) surface in a  $p(2 \times 2)$  cell for a  $\mathbf{k}$ -point grid ranging between  $(6 \times 6 \times 1)$  and  $(24 \times 24 \times 1)$ . From this follows for a calculation with a  $(4 \times 4 \times 1)$ - $\mathbf{k}$ -point grid in the  $p(6 \times 6)$  cell, respectively a  $(12 \times 12 \times 1)$ - $\mathbf{k}$ -point grid in an  $p(2 \times 2)$  cell an error of  $\Delta E_{\text{kpoints}} = 2 \text{ meV}$  and  $\Delta \mu_{\text{kpoints}} = 1.2 \text{ meÅ}$ .

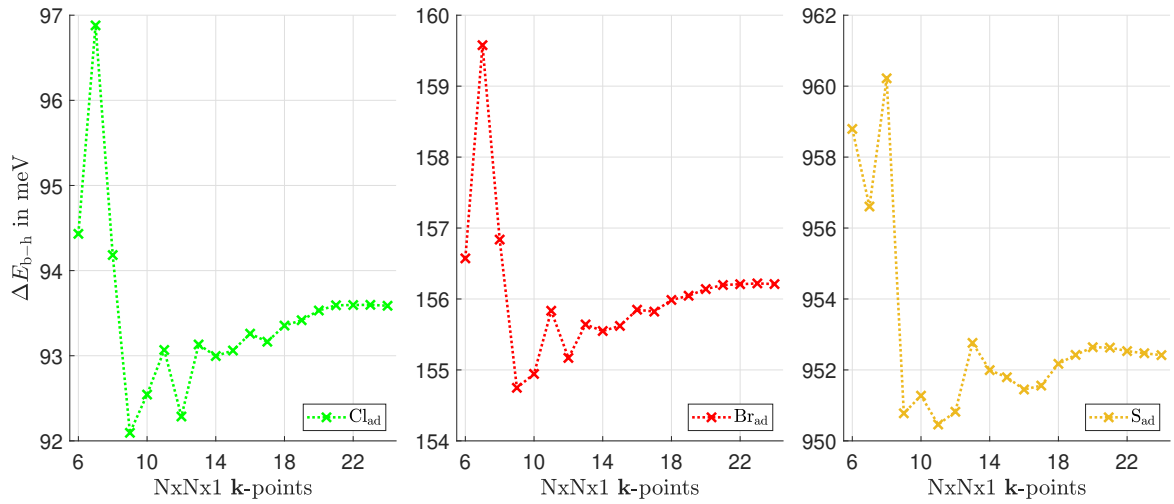


Figure S7: Difference of the energy of  $\text{Cl}_{\text{ad}}$ ,  $\text{Br}_{\text{ad}}$  and  $\text{S}_{\text{ad}}$  between hollow and bridge position depending on the  $\mathbf{k}$ -point grid.

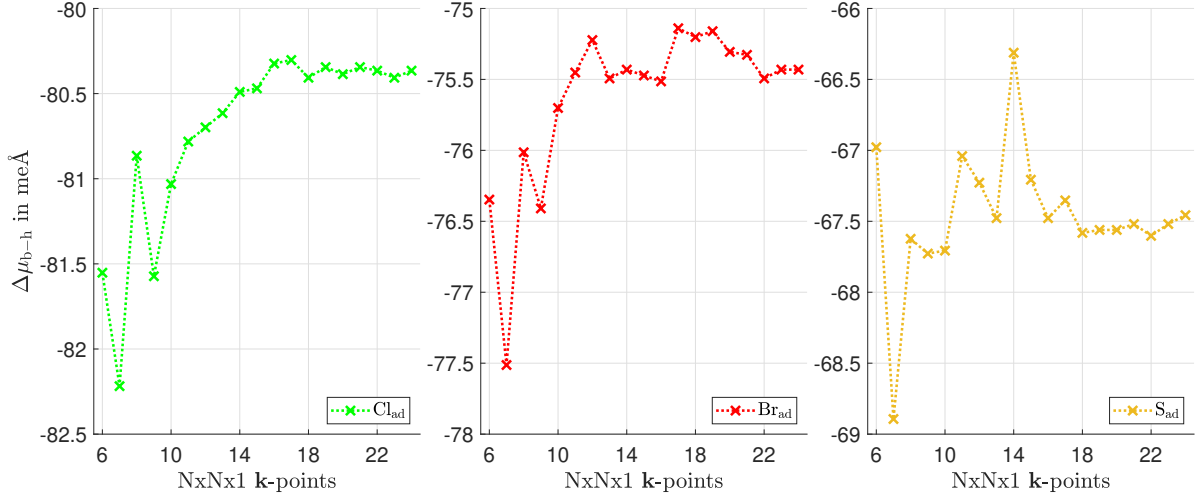


Figure S8: Difference of the dipole moment of  $\text{Cl}_{\text{ad}}$ ,  $\text{Br}_{\text{ad}}$  and  $\text{S}_{\text{ad}}$  between hollow and bridge position depending on the  $\mathbf{k}$ -point grid.

### 1.5 Threshold for residual force orthogonal to the diffusion path

For the NEB calculations it is important to set a limit as to how small the residual force orthogonal to the diffusion path has to be, so that the calculation is assumed to have converged. In the NEB calculations for the diffusion paths,  $0.05 \text{ eV}/\text{\AA}$  was used. A lower threshold has little effect on the activation barrier for diffusion pathways as shown in Figure S9. In this Figure the largest remaining norm of the force orthogonal to the diffusion path on an image for successive iterations of a single CI-NEB run is plotted versus the activation energy for the rotation diffusion path of  $\text{S}_{\text{ad}}$  on the  $c(2 \times 2)$ -Cl covered  $\text{Cu}(100)$  surface in a  $p(6 \times 6)$  surface unit cell (see section 3). The result for the activation energy varies by less than  $\Delta E_{\text{path}} = 2 \text{ meV}$  when the threshold for the residual force orthogonal to the path is lowered.

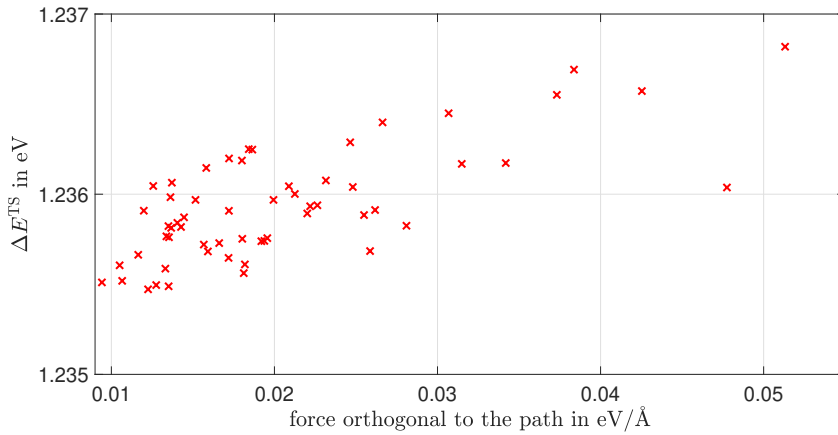


Figure S9: Activation energy  $\Delta E^{\text{TS}}$  plotted versus the largest value of the norm of the force orthogonal to the diffusion path of  $\text{S}_{\text{ad}}$  on the  $c(2 \times 2)$ -Cl covered  $\text{Cu}(100)$  surface (see section 3).

Table S2: Adsorption energy  $\Delta E_{\text{ads}}$  per atom with reference to 1/2 times the energy of the respective molecule ( $\text{Cl}_2$ ,  $\text{Br}_2$  or  $\text{S}_2$ ) at hollow and bridge site of the Cu(100) substrate surface, energy difference  $\Delta E_{\text{b-h}}$  of  $\text{Cl}_{\text{ad}}$ ,  $\text{Br}_{\text{ad}}$  or  $\text{S}_{\text{ad}}$  on the Cu(100)-surface between bridge and hollow site for adsorbate coverage  $\Theta = 0.25$  ( $\text{p}(2 \times 2)$ ) as well as the dipole moment differences  $\Delta \mu_{\text{b-h}}$  and the change of  $z$ -coordinate  $\Delta z_{\text{b-h}}$ .

|                                      | $\text{Cl}_{\text{ad}}$                          | $\text{Br}_{\text{ad}}$  | $\text{S}_{\text{ad}}$                              |
|--------------------------------------|--|--|---|
| $\Delta E_{\text{ads}}$ hollow in eV | 1.93   | 1.86<br>[1.98] <sup>a</sup>  | 2.44<br>[2.11] <sup>b</sup><br>[2.475] <sup>c</sup> |
| $\Delta E_{\text{ads}}$ bridge in eV | 1.85   | 1.71<br>[1.83] <sup>a</sup>  | 1.48<br>[1.23] <sup>b</sup>                         |
| $\Delta E_{\text{b-h}}$ in eV        | 0.09   | 0.15<br>[0.15] <sup>a</sup>  | 0.96<br>[0.881] <sup>b</sup>                        |
|                                      | [0.12] <sup>d</sup>                              | [0.19] <sup>d</sup>  |   |
|                                      | [0.06] <sup>e</sup>                              | [0.13] <sup>e</sup>  |   |
| $\Delta \mu_{\text{b-h}}$ in meÅ     | -82<br>[-49] <sup>d</sup><br>[-100] <sup>e</sup> | -77<br>[-44] <sup>d</sup><br>[-103] <sup>e</sup>                         | -68   |
| $\Delta z_{\text{b-h}}$ in mÅ        | 251±20   | 223±20<br>[190] <sup>a</sup><br>[164] <sup>d</sup><br>[245] <sup>e</sup> | 319±20  |

<sup>a</sup> by Kenny *et al.* in a  $\text{p}(2 \times 2)$  cell [14].

<sup>b</sup> RPBE by Bernard Rodríguez *et al.* in a  $\text{p}(2 \times 2)$  cell [1].

<sup>c</sup> RPBE by Bradley *et al.* in a  $\text{p}(2 \times 2)$  cell [2].

<sup>d</sup> PW91 by Rahn *et al.* in a  $\text{c}(2 \times 2)$  cell [25].

<sup>e</sup> PW91 by Rahn *et al.* in a  $\text{c}(6 \times 6)$  cell [25].

As mentioned in the main paper, in case of  $\text{S}_{\text{ad}}$  and  $\text{CH}_3\text{S}_{\text{ad}}$  diffusion paths with a larger number of adsorbate adatoms dislocated along the diffusion path the uncertainties will be larger than for above simple configurations in particular due to the problematic convergence with layer thickness, the authors of Ref. [25] obtain an uncertainty of  $\pm 0.1$  eV for the energy barrier.

## 2 $\text{CH}_3\text{S}_{\text{ad}}$ diffusion on Cu(100) without halogen co-adsorbates

As noted in the main paper, the energy barrier for the diffusion of  $\text{S}_{\text{ad}}$  is significantly higher than the energy barrier of  $\text{CH}_3\text{S}_{\text{ad}}$  on the Cu(100) surface without co-adsorbates. This has been rationalized by the tilting of the S–C-bond with respect to the surface along the diffusion path.

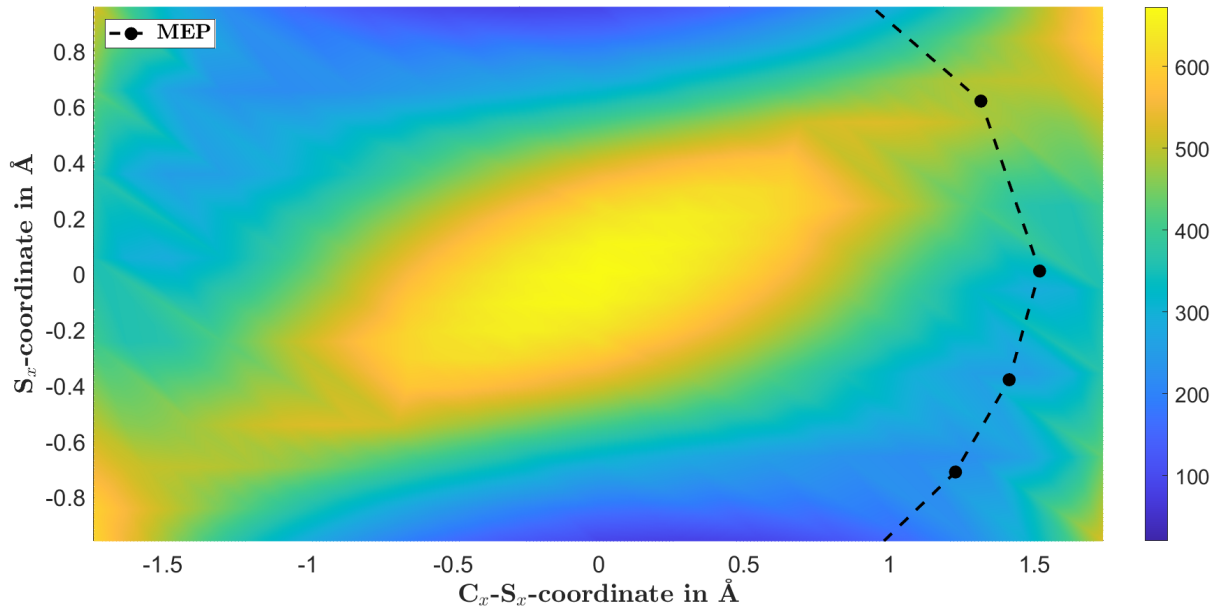


Figure S10: Energy difference with reference to the adsorption geometry as a function of the  $x$ -coordinate of the sulfur  $S_x$  and the tilt of the thiolate, described by the  $C_x - S_x$  coordinate difference. Minimum energy pathway (MEP) denoted by dashed line. Coordinates refer to the bridge position of the substrate. The colorscale indicates the energy difference in meV.

The tilting of the S–C-bond in the transition state can also be seen by mapping the energy of  $\text{CH}_3\text{S}_{\text{ad}}$  versus the  $x$ -coordinate of the sulfur atom (with respect to the bridge position) and the difference of  $x$ -coordinate of the carbon and the sulfur atom. The result is shown in Figure S10. Every combination of a  $S_x$ - and a  $C_x$ -coordinate corresponds to a position along the diffusion path and a tilt angle. The energy of the configurations have been calculated in a  $p(3 \times 3)$  surface unit cell with four Cu layers and a  $4 \times 4 \times 1$   $\mathbf{k}$ -point grid [20]. The energy surface has been interpolated. The energy reference is the adsorption energy of  $\text{CH}_3\text{S}_{\text{ad}}$  at the Cu(100) hollow site. The energy surface confirms the diffusion path calculated with the NEB method [13, 19, 26] (MEP) and, in particular, the position of the transition state.

In Figure S11 the configurations along the minimum energy path for  $\text{CH}_3\text{S}_{\text{ad}}$  on the Cu(100) without co-adsorbates are shown.

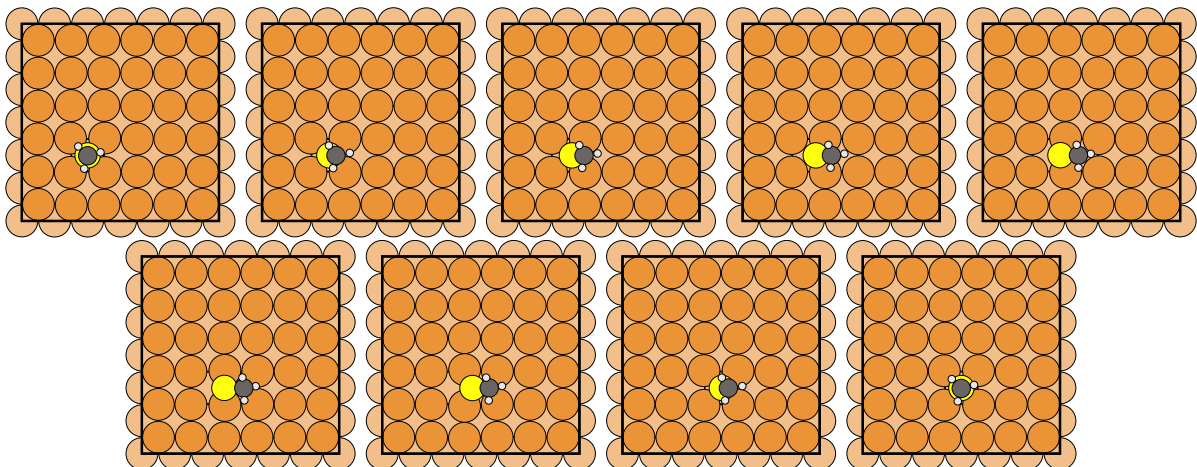


Figure S11: Diffusion path for  $\text{CH}_3\text{S}_{\text{ad}}$  on the  $\text{Cu}(100)$  surface without co-adsorbates.

### 3 Comparison of rotation path of $\text{S}_{\text{ad}}$ with Rahn et al.

Rahn *et al.* have calculated diffusion paths for  $\text{S}_{\text{ad}}$  on the  $\text{Cu}(100)$  surface in the presence of a  $c(2\times 2)$ -Cl or  $c(2\times 2)$ -Br adlayer, with one halogen atom substituted by the  $\text{S}_{\text{ad}}$  [24]. In their rotation diffusion path, the  $\text{S}_{\text{ad}}$  and the co-adsorbates change places roughly within a circle. Since a similar diffusion path is conceivable for  $\text{CH}_3\text{S}_{\text{ad}}$ , we have started from this path by Rahn *et al.* We have reproduced their result within the estimated accuracy. Differences in the computational approaches are listed in Table S3.

Table S3: Computational details and results for the rotation diffusion path of  $\text{S}_{\text{ad}}$  on a  $c(2\times 2)$ -Cl or  $c(2\times 2)$ -Br covered  $\text{Cu}(100)$  surface for our calculations and the calculations by Rahn *et al.* [24].

|   | own calculations                  | Rahn <i>et al.</i> [24, 25]        |
|---|-----------------------------------|------------------------------------|
| Computational Software                        | Quantum ESPRESSO [12, 11]         | VASP [16, 17, 15]                  |
| Pseudopotentials                              | USPP [4, 10, 23]                  | PAW [18]                           |
| XC-functional                                 | PBE [21]                          | PW91 [22]                          |
| Cut-off energy                                | 476 eV                            | 260 eV                             |
| Vacuum in Å                                   | 16                                | 14                                 |
| <b>k</b> -point grid [20]                     | $4\times 4\times 1$               | $3\times 3\times 1$                |
| path threshold                                | $0.05 \frac{\text{eV}}{\text{Å}}$ | $0.005 \frac{\text{eV}}{\text{Å}}$ |
| $\Delta E_1^{\text{Cl}}$ in eV <sup>a</sup>   | 1.24                              | 1.21                               |
| $\Delta E_2^{\text{Cl}}$ in eV <sup>b</sup>   | 1.22                              | 1.29                               |
| $\Delta E^{\text{Br}}$ in eV                  | 1.57                              | 1.64                               |
| $\Delta \mu_1^{\text{Cl}}$ in eÅ <sup>c</sup> | -0.10                             | -0.09                              |
| $\Delta \mu_2^{\text{Cl}}$ in eÅ <sup>d</sup> | -0.30                             | -0.28                              |
| $\Delta \mu^{\text{Br}}$ in eÅ                | -0.27                             | -0.26                              |

<sup>a</sup>  $\Delta E_1^{\text{Cl}}$  refers to the change in energy at scaled reaction coordinate 0.12.

<sup>b</sup>  $\Delta E_2^{\text{Cl}}$  refers to the change in energy at scaled reaction coordinate 0.5.

<sup>c</sup>  $\Delta \mu_1^{\text{Cl}}$  refers to the change in dipole moment at scaled reaction coordinate 0.12.

<sup>d</sup>  $\Delta \mu_2^{\text{Cl}}$  refers to the change in dipole moment at scaled reaction coordinate 0.5.

There are several local energy maxima along the diffusion path. The largest denotes the (overall) transition state. Due to the small energy difference between these local maxima, the geometry of the transition state with highest potential energy comes out differently in the path of  $S_{\text{ad}}$  on a  $c(2\times 2)$ -Cl covered Cu(100) surface calculated here and the calculation by Rahn *et al.* [24] (Figure S12). In the calculation by Rahn *et al.* [24], the transition state is at the scaled reaction coordinate 0.5, while in our calculation the transition state is at the scaled reaction coordinate 0.12. The difference of energy and dipole moment between the adsorption state and the transition state are listed in Table S3.

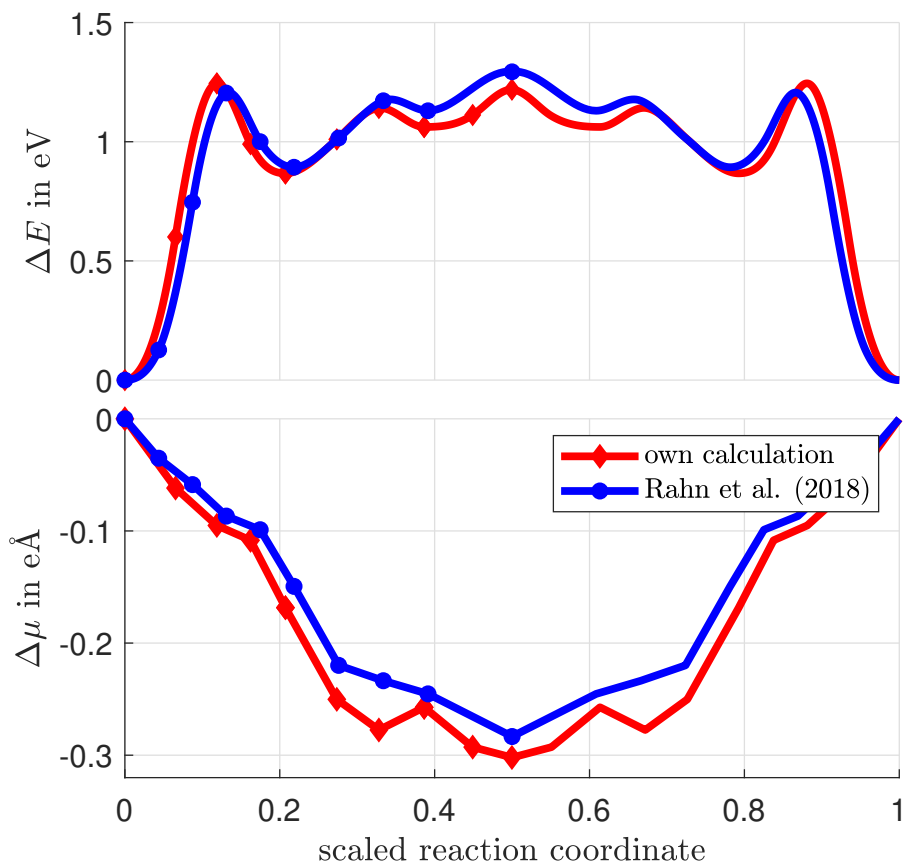


Figure S12: Variation of energy and dipole moment as a function of the scaled reaction coordinate along the rotation diffusion path in comparison to the calculation by Rahn *et al.* [24] in case of the diffusion of sulfur on the Cu(100) surface with a  $c(2\times 2)$ -Cl coverage.

The rotation diffusion path of  $S_{\text{ad}}$  on the  $c(2\times 2)$ -Br covered Cu(100) surface from Rahn *et al.* [24] has also been reproduced within the estimated accuracy and there are no differences in the location of the transition state (Figure S13). The differences of energy and dipole moment between adsorption state and transition state are listed in Table S3.

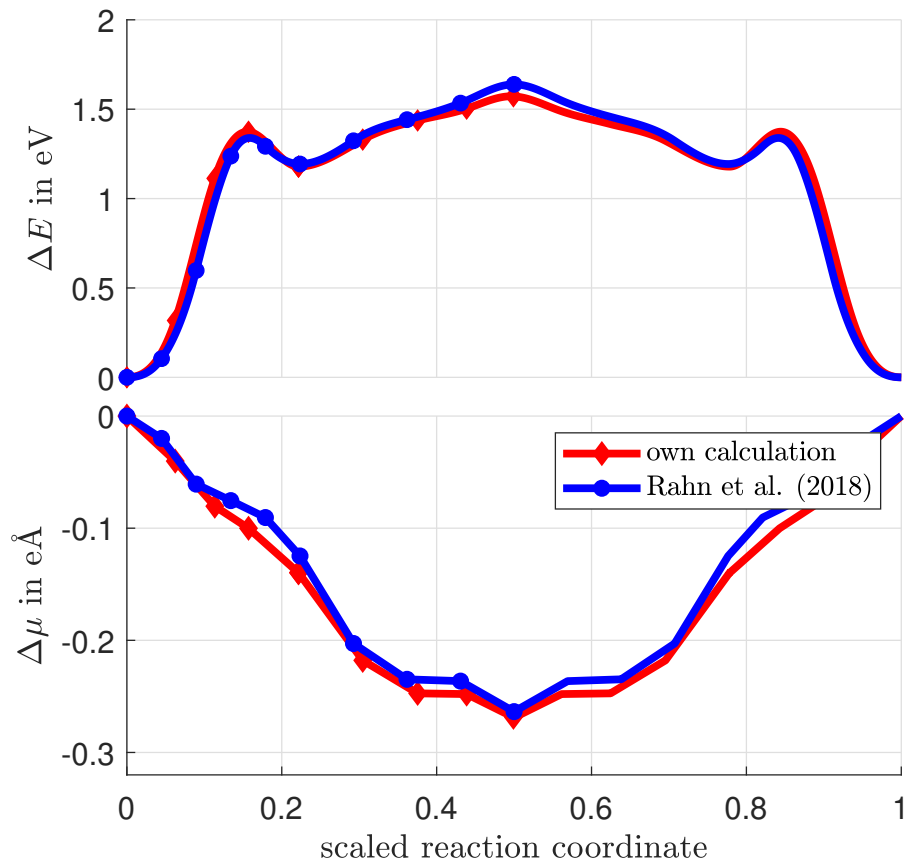


Figure S13: Variation of energy and dipole moment as a function of the scaled reaction coordinate along the diffusion path and comparison with the calculations by Rahn *et al.* [24] for the diffusion of sulfur on the Cu(100) surface with a  $c(2 \times 2)$ -Br coverage.

#### 4 Diffusion paths for $S_{ad}$ and $CH_3S_{ad}$ on a halogen covered Cu(100) surface

The rotation diffusion paths for  $CH_3S_{ad}$  on the Cu(100) surface with a  $c(2 \times 2)$ -Cl or -Br adlayer are shown in Figures S14 and S15. In Figure S16 the change in energy, the change in dipole moment, the change of the  $z$ -coordinate of the S atom and the sum of change of  $z$ -coordinates of all halogen atoms along the rotation diffusion path are shown for  $S_{ad}$  and  $CH_3S_{ad}$ .

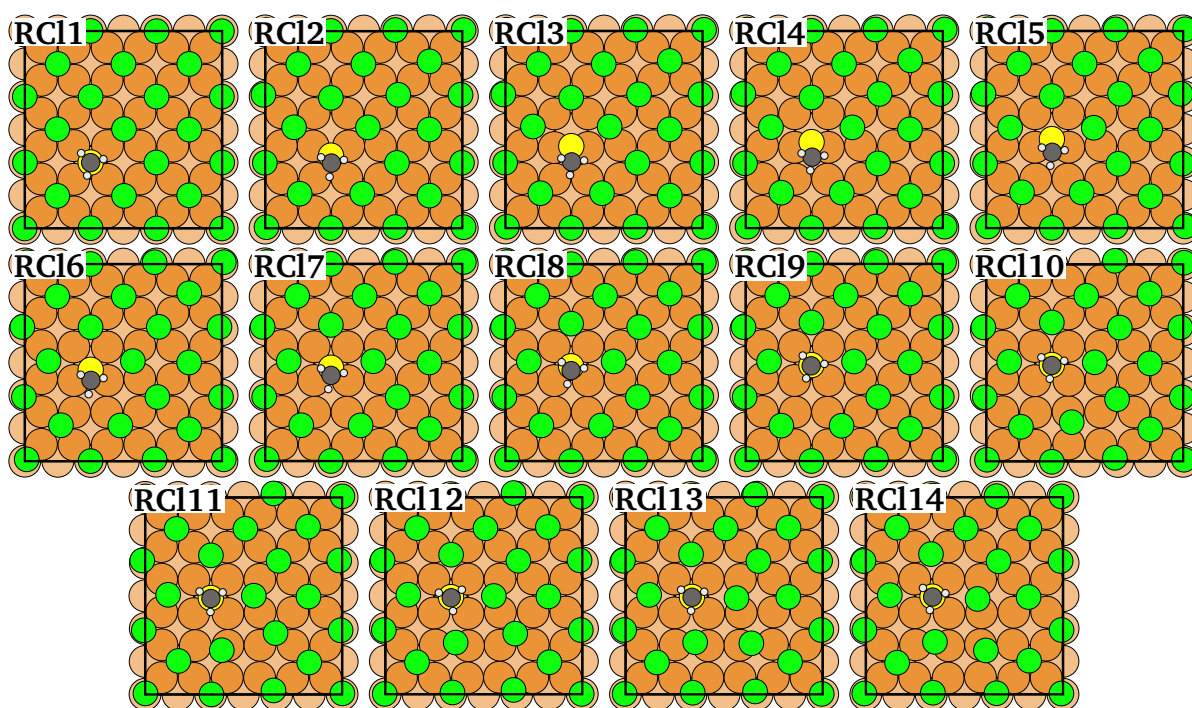


Figure S14: First half of the rotation diffusion path for  $\text{CH}_3\text{S}_{\text{ad}}$  on a  $\text{Cu}(100)$  surface with a  $c(2 \times 2)$ -Cl adlayer. The second half can be obtained by applying a mirror operation. The complete path is shown in a video attached to the ESI.

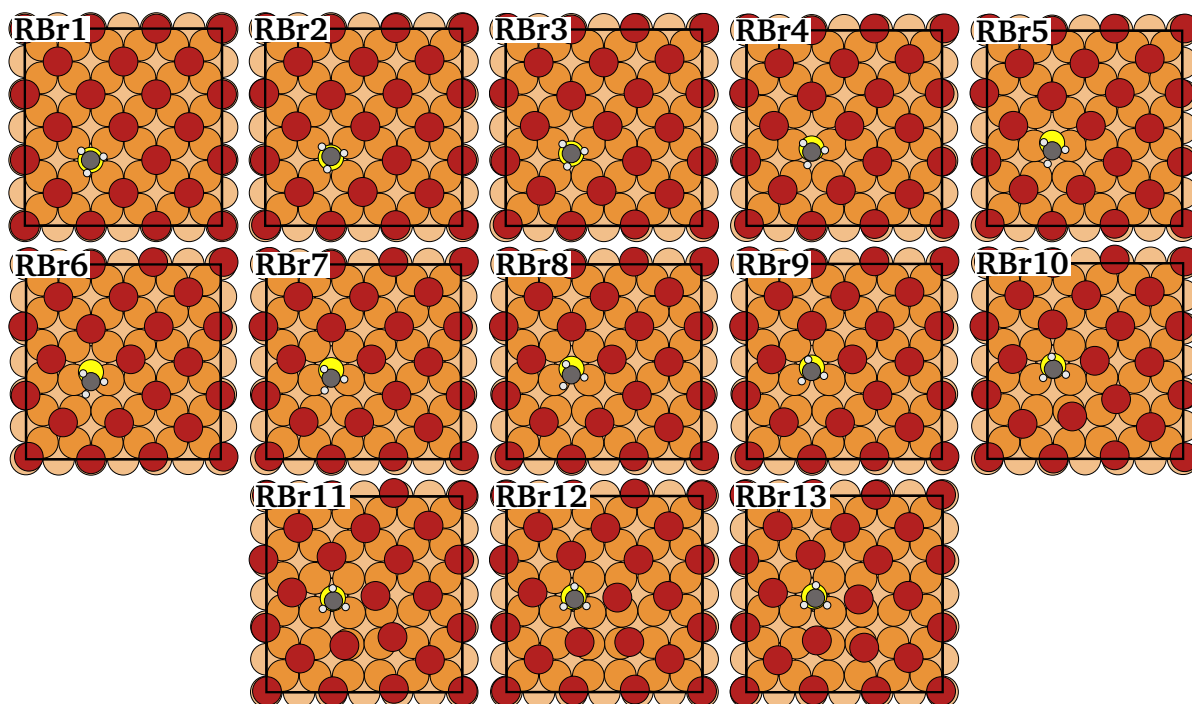


Figure S15: First half of the rotation diffusion path for  $\text{CH}_3\text{S}_{\text{ad}}$  on a  $\text{Cu}(100)$  surface with a  $c(2 \times 2)$ -Br adlayer. The second half can be obtained by applying a mirror operation.

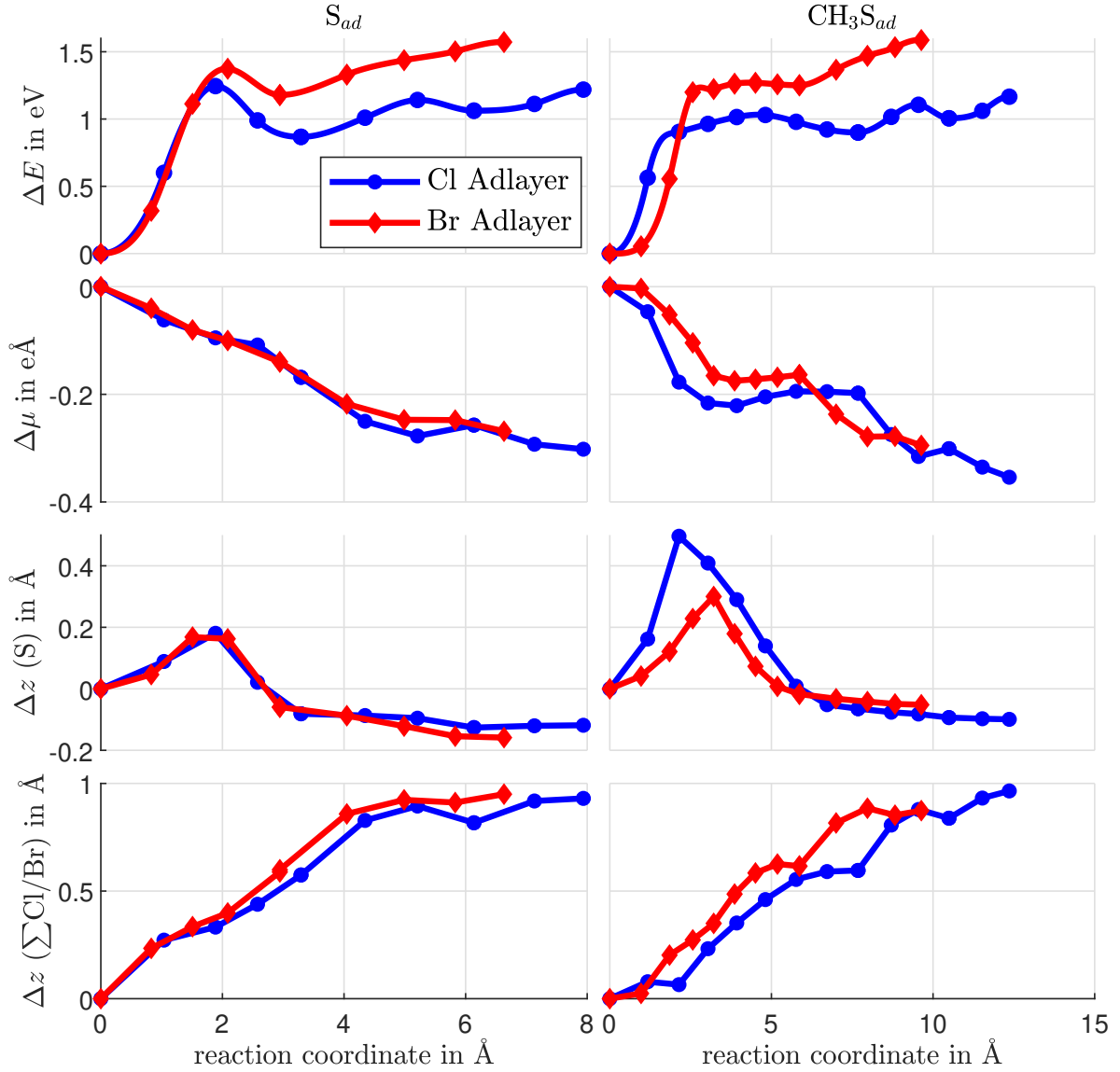


Figure S16: Comparison between the rotation diffusion paths for  $S_{ad}$  and  $CH_3S_{ad}$  on a halogen covered Cu(100) surface. From top to bottom is the change in energy  $\Delta E$ , the change in dipole moment  $\Delta\mu$ , the change of the  $z$ -coordinate of the S atom and the sum of change of  $z$ -coordinates of all halogen atoms along the diffusion path.

Note: Only the first half of the reaction path is shown. The second half can be obtained by applying a suitable mirror operation.

For comparison the diffusion paths I and II for  $S_{ad}$  on the Cu(100) surface with a vacancy in the  $c(2\times 2)$ -Cl or -Br adlayer are shown in Figures S17 to S20. In Figure S21 the change in energy, the change in dipole moment, the change of the  $z$ -coordinate of the S atom and the sum of change of  $z$ -coordinates of all halogen atoms along the diffusion paths I and II for  $S_{ad}$  are shown. Note that vacancy assisted diffusion paths for the  $S_{ad}$  have also already been calculated by Deuchler and Stremme [25].

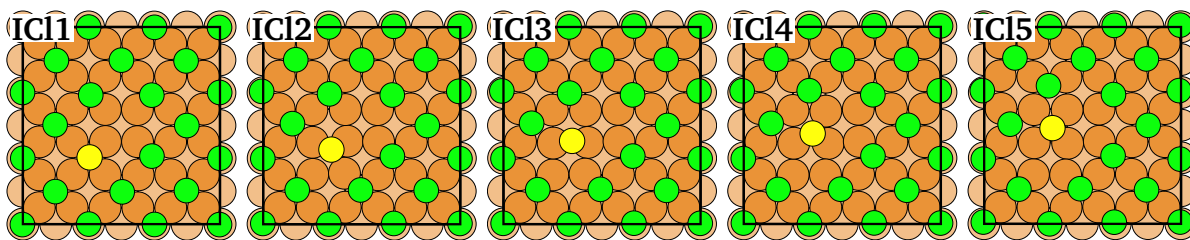


Figure S17: First half of the diffusion path I for  $S_{ad}$  on a Cu(100) surface with a  $c(2 \times 2)$ -Cl adlayer and a vacancy therein. The second half can be obtained by applying a mirror operation. The complete path is shown in a video attached to the ESI.

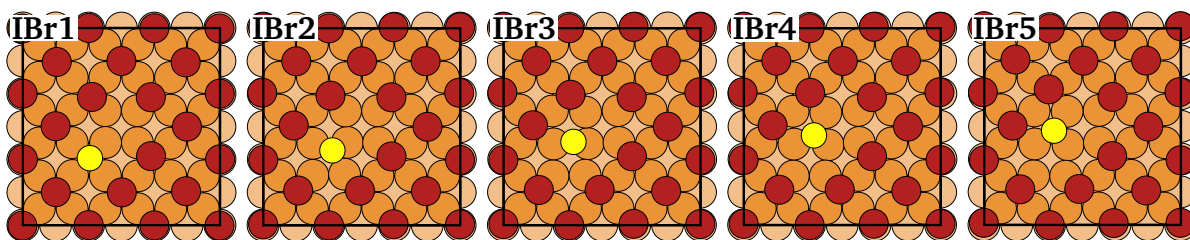


Figure S18: First half of the diffusion path I for  $S_{ad}$  on a Cu(100) surface with a  $c(2 \times 2)$ -Br adlayer and a vacancy therein. The second half can be obtained by applying a mirror operation.

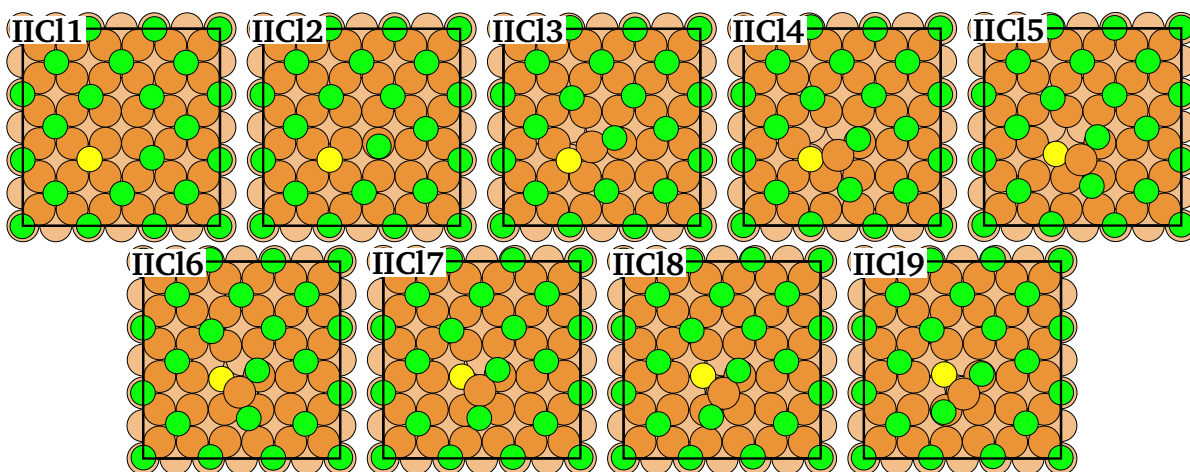


Figure S19: First half of the diffusion path II for  $S_{ad}$  on a Cu(100) surface with a  $c(2 \times 2)$ -Cl adlayer and a vacancy therein. The second half can be obtained by applying a mirror operation. The complete path is shown in a video attached to the ESI.

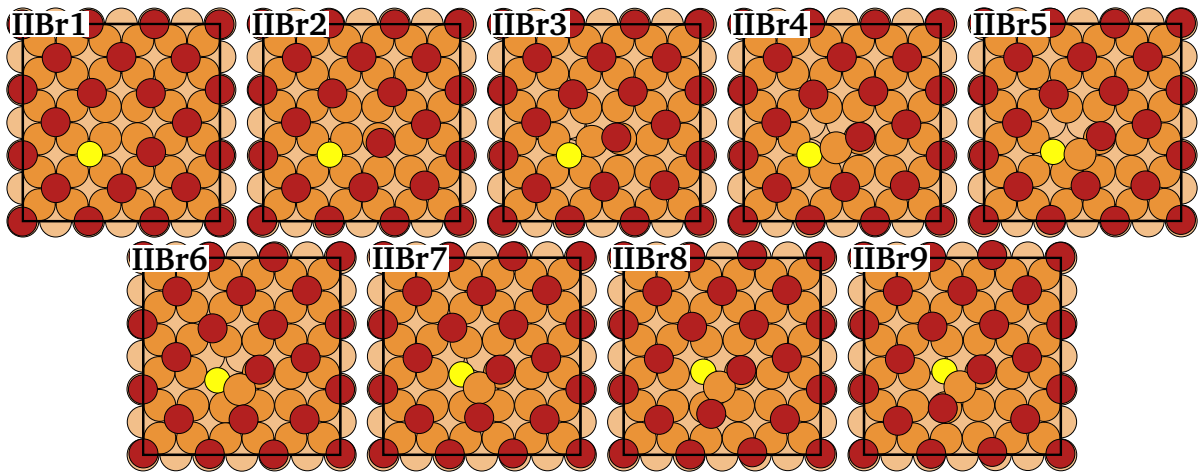


Figure S20: First half of the diffusion path II for  $S_{ad}$  on a Cu(100) surface with a  $c(2 \times 2)$ -Br adlayer and a vacancy therein. The second half can be obtained by applying a mirror operation.

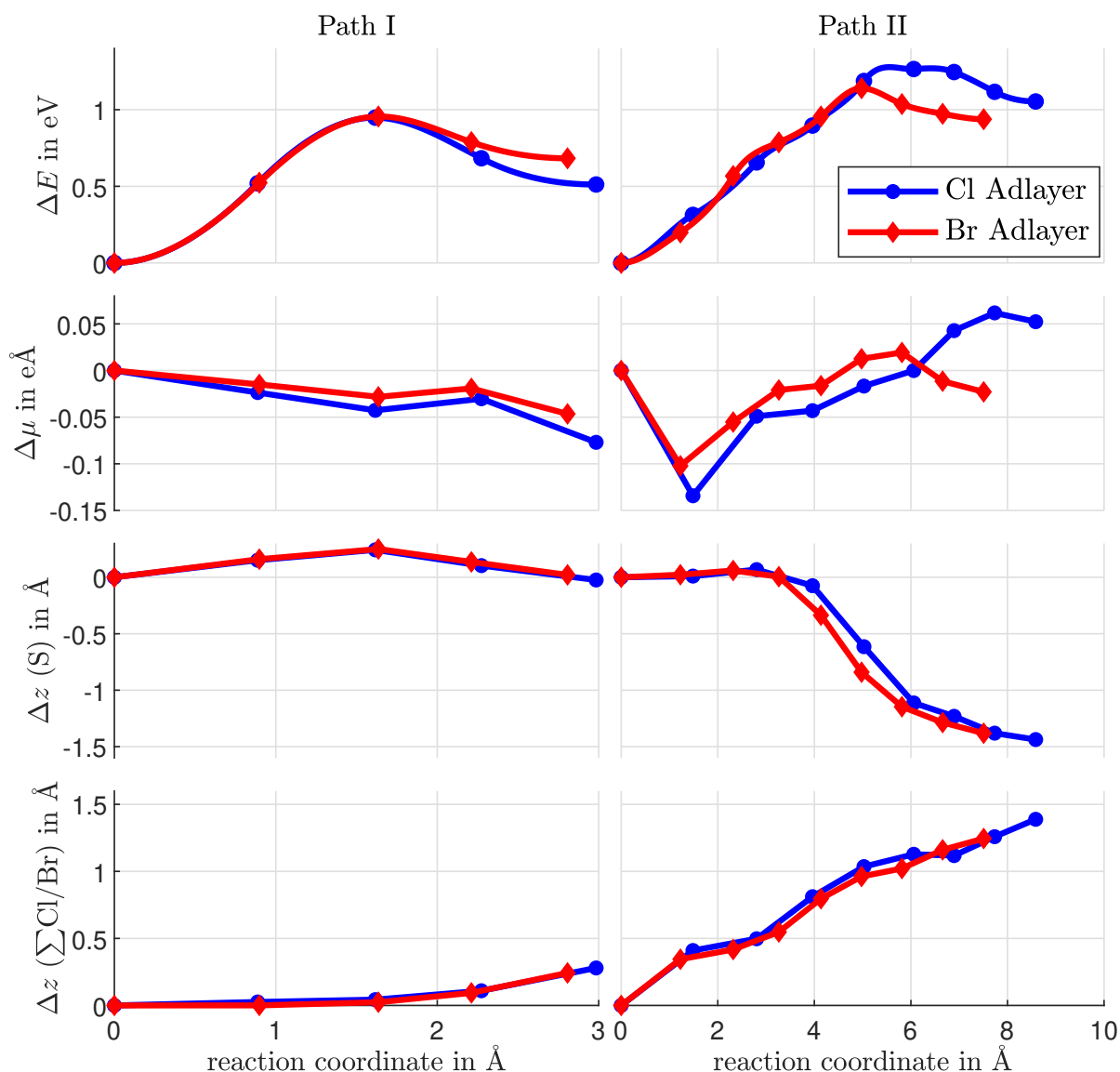


Figure S21: Diffusion paths I and II for  $S_{\text{ad}}$  on a halogen covered Cu(100) surface with a vacancy. From top to bottom is the change in energy  $\Delta E$ , the change in dipole moment  $\Delta\mu$ , the change of the  $z$ -coordinate of the S atom and the sum of change of  $z$ -coordinates of all halogen atoms along the diffusion path. Note: Only the first half of the reaction path is shown. The second half can be obtained by applying a suitable mirror operation.

The diffusion paths A, B and C for  $\text{CH}_3S_{\text{ad}}$  on the Cu(100) surface with a vacancy in the  $c(2\times 2)$ -Cl or -Br adlayer are shown in Figures S22 to S27. In Figure S28 the change in energy, the change in dipole moment, the change of the  $z$ -coordinate of the S atom and the sum of change of  $z$ -coordinates of all halogen atoms along the diffusion paths A, B and C for  $\text{CH}_3S_{\text{ad}}$  are shown.

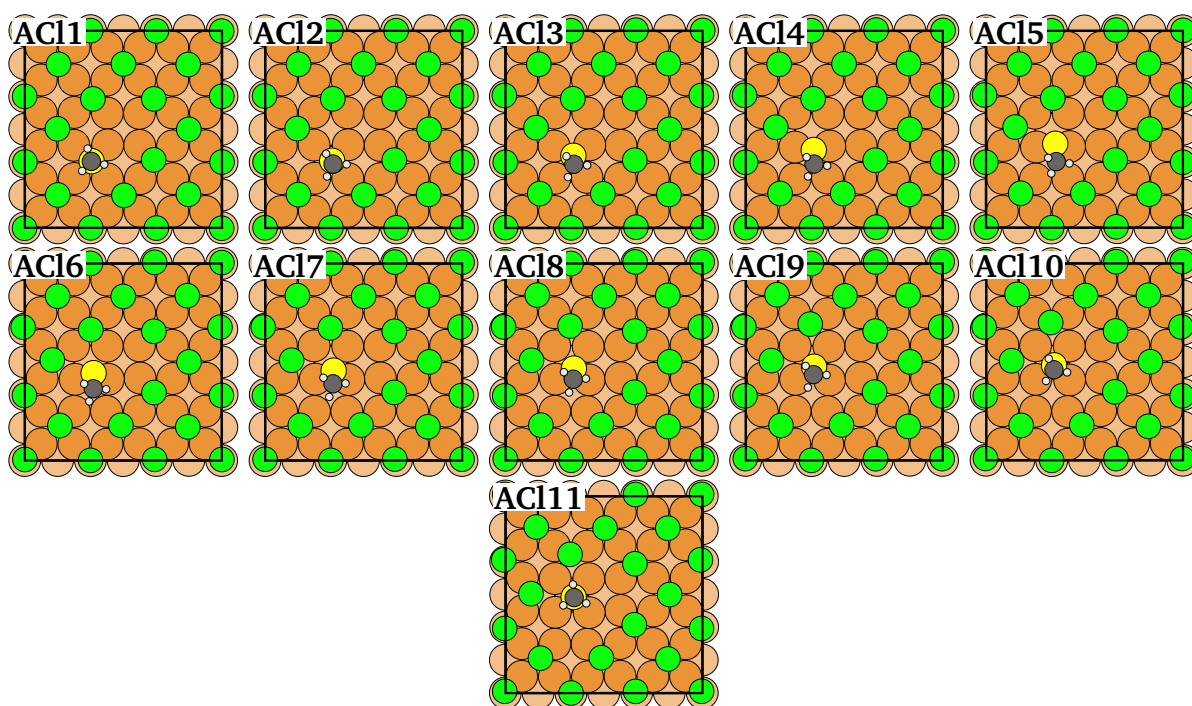


Figure S22: First half of the diffusion path A for  $\text{CH}_3\text{S}_{\text{ad}}$  on a Cu(100) surface with a  $c(2\times 2)$ -Cl adlayer and a vacancy therein. The second half can be obtained by applying a mirror operation. The complete path is shown in a video attached to the ESI.

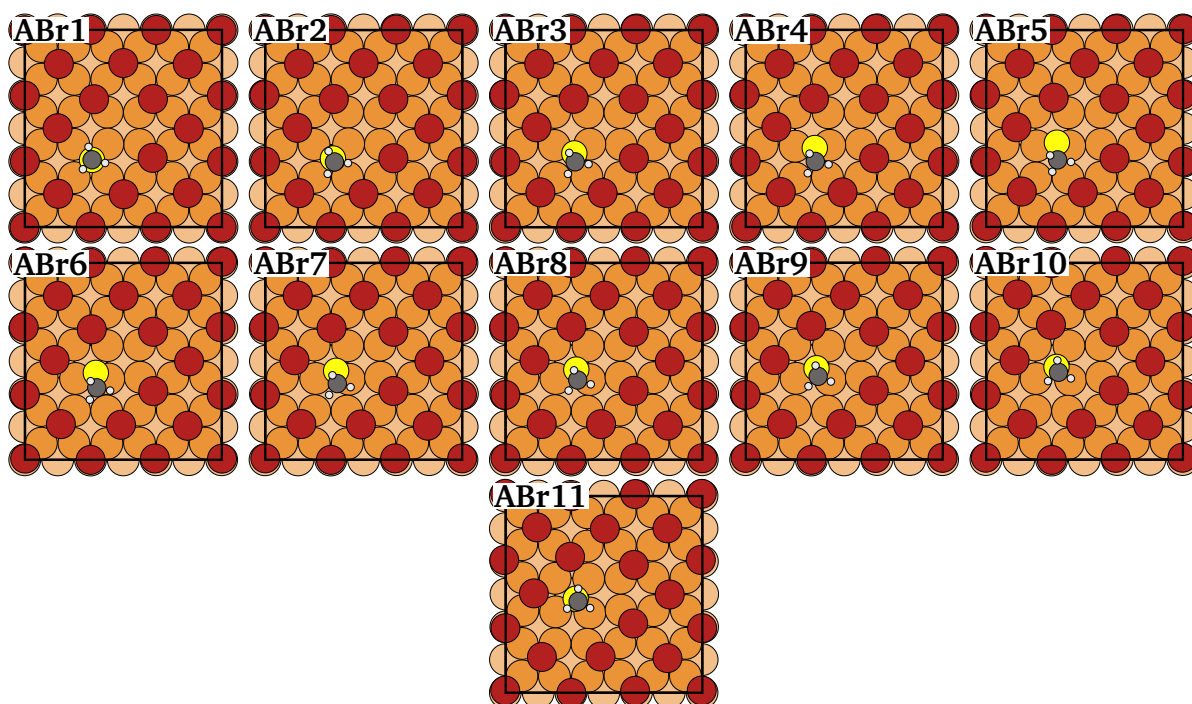


Figure S23: First half of the diffusion path A for  $\text{CH}_3\text{S}_{\text{ad}}$  on a Cu(100) surface with a  $c(2\times 2)$ -Br adlayer and a vacancy therein. The second half can be obtained by applying a mirror operation.

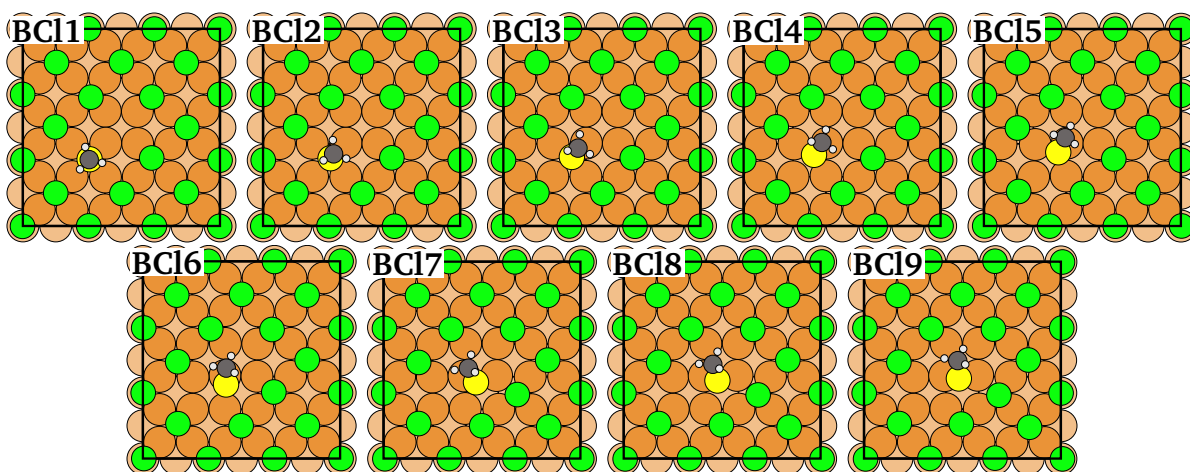


Figure S24: First part of the diffusion path B for  $\text{CH}_3\text{S}_{\text{ad}}$  on a Cu(100) surface with a  $c(2\times 2)$ -Cl adlayer and a vacancy therein. The second part is equivalent to the first part (ACl1 to ACl5) of path A. The complete path is shown in a video attached to the ESI.

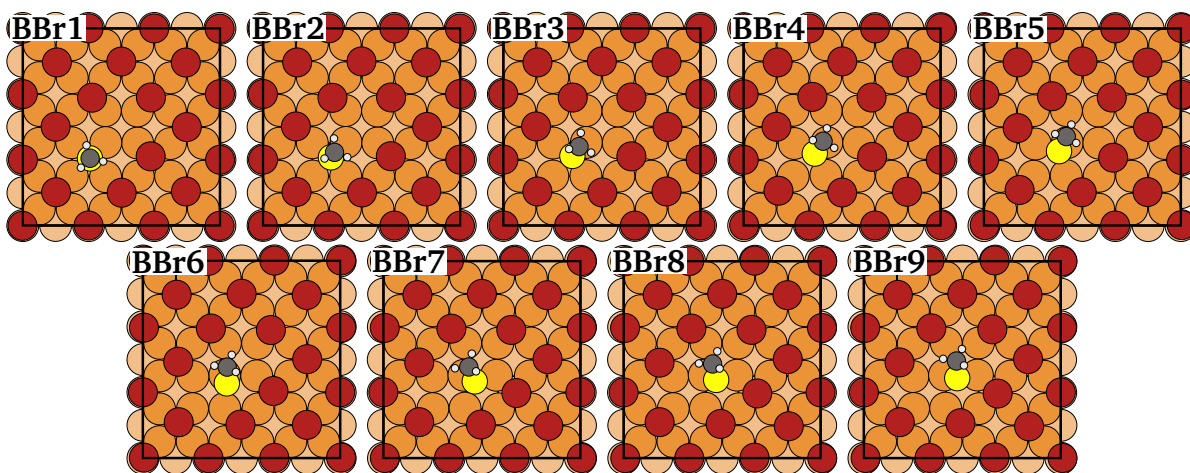


Figure S25: First part of the diffusion path B for  $\text{CH}_3\text{S}_{\text{ad}}$  on a Cu(100) surface with a  $c(2\times 2)$ -Br adlayer and a vacancy therein. The second part is equivalent to the first part (ABr1 to ABr5) of path A.

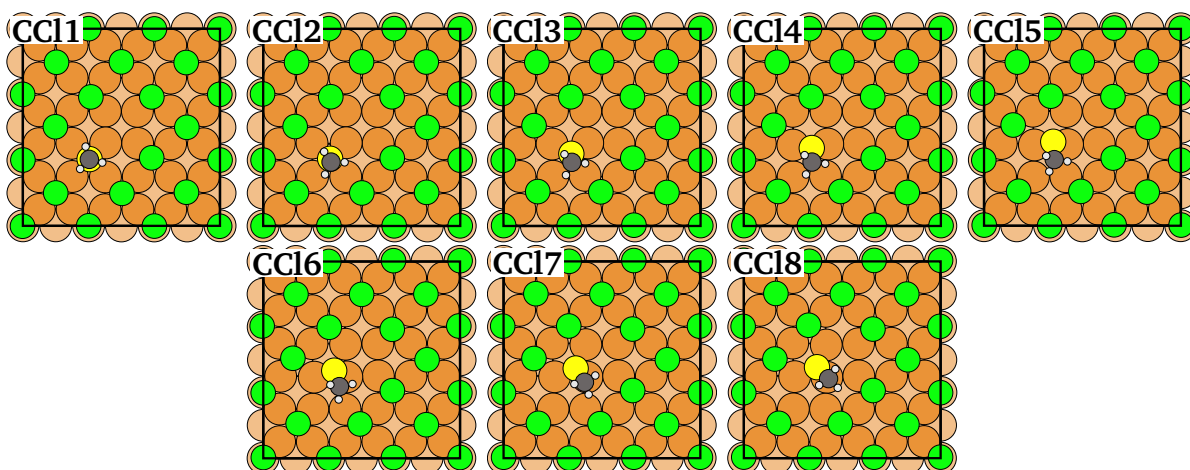


Figure S26: First half of the diffusion path C for  $\text{CH}_3\text{S}_{\text{ad}}$  on a Cu(100) surface with a  $c(2\times 2)$ -Cl adlayer and a vacancy therein. The second half can be obtained by applying a mirror operation. The complete path is shown in a video attached to the ESI.

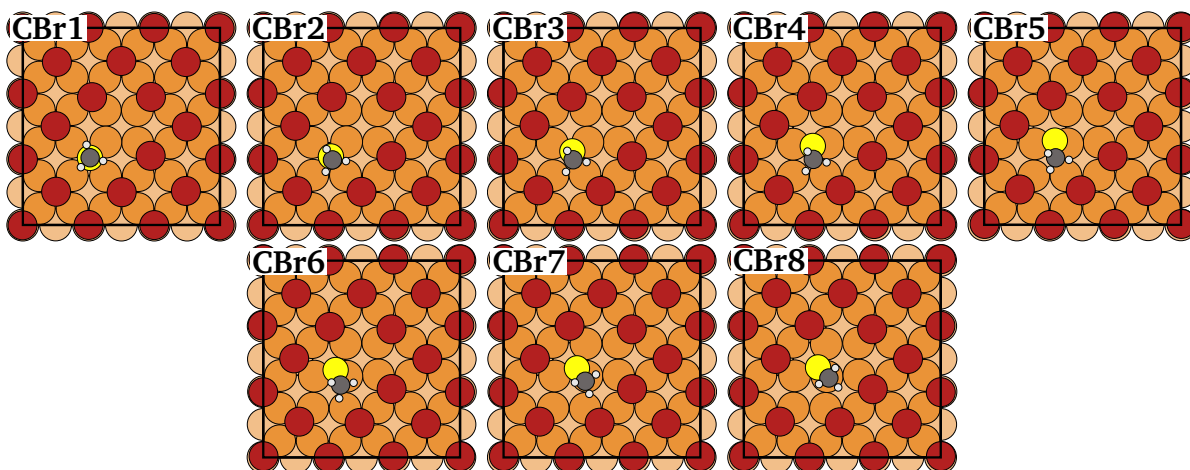


Figure S27: First half of the diffusion path C for  $\text{CH}_3\text{S}_{\text{ad}}$  on a Cu(100) surface with a  $c(2\times 2)$ -Br adlayer and a vacancy therein. The second half can be obtained by applying a mirror operation.

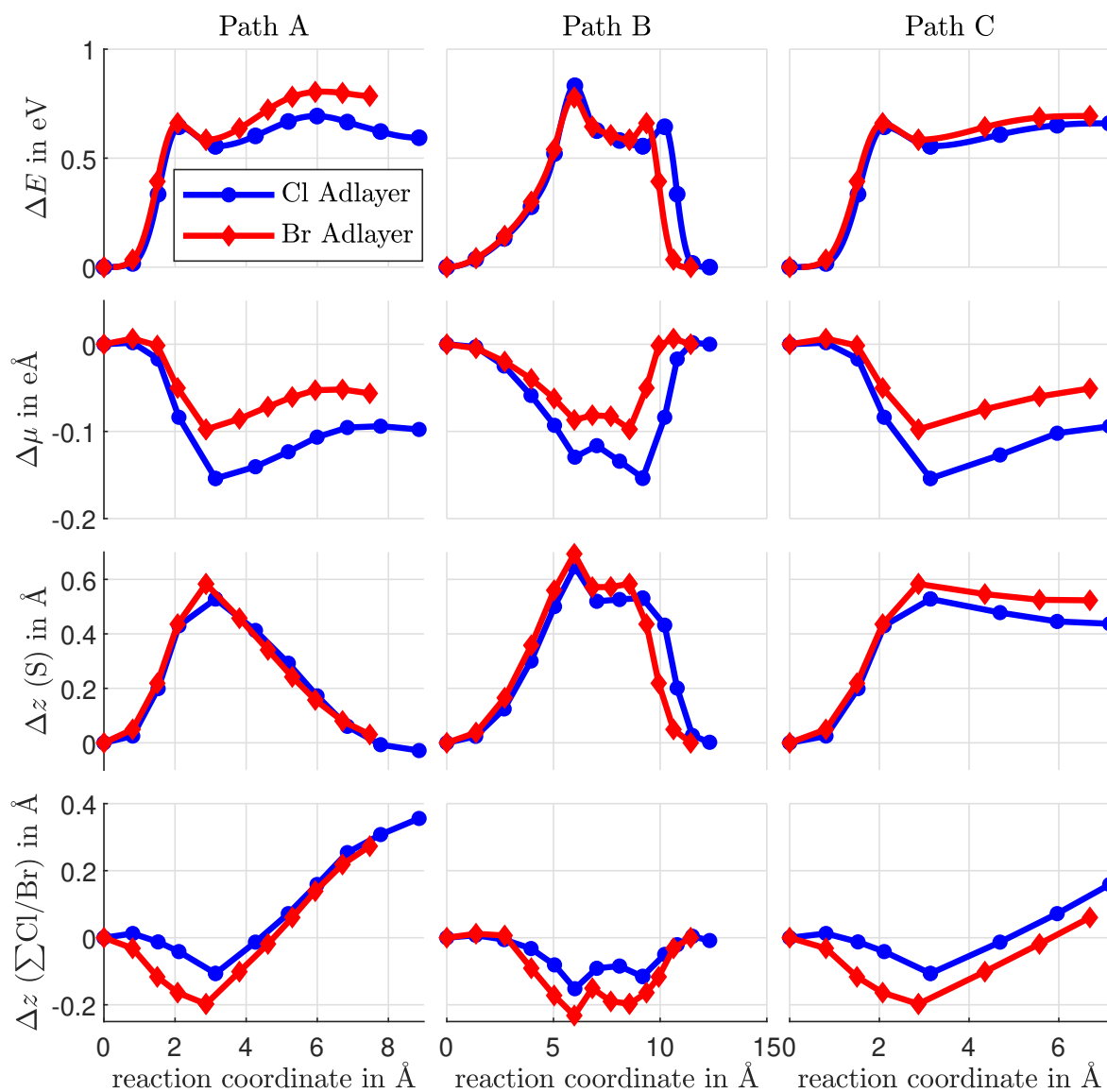


Figure S28: Comparison between the diffusion paths A, B and C for  $\text{CH}_3\text{S}_{\text{ad}}$  on a halogen covered  $\text{Cu}(100)$  surface with a vacancy. From top to bottom is the change in energy  $\Delta E$ , the change in dipole moment  $\Delta\mu$ , the change of the  $z$ -coordinate of the S atom and the sum of change of  $z$ -coordinates of all halogen atoms along the diffusion path.

Note: For the paths A and C only the first half of the reaction path is shown. The second half can be obtained by applying a suitable mirror operation. Path B is shown in full.

## Acknowledgments

We are grateful to O. Magnussen for pointing out the diffusion systems to us and sharing his insights and to L. Deuchler for providing his DFT data for  $\text{S}_{\text{ad}}$  diffusion on halogen covered  $\text{Cu}(100)$ . Helpful discussions with S. Buttenschön and M. Funk are gratefully

acknowledged. This research was supported in part through high-performance computing resources available at the Kiel University Computing Centre.

## References

- [1] C. R. Bernard Rodríguez and J. A. Santana. Adsorption and diffusion of sulfur on the (111), (100), (110), and (211) surfaces of FCC metals: Density functional theory calculations. *The Journal of Chemical Physics*, 149(20):204701, 11 2018.
- [2] M. Bradley, D. Woodruff, and J. Robinson. Adsorbate-induced surface stress, surface strain and surface reconstruction: S on Cu(100) and Ni(100). *Surface Science*, 613:21–27, 2013.
- [3] A. Dal Corso. Pseudopotential hydrogen: H.pbe-rrkjus.upf, 2008. [http://pseudopotentials.quantum-espresso.org/upf\\_files/H.pbe-rrkjus.UPF](http://pseudopotentials.quantum-espresso.org/upf_files/H.pbe-rrkjus.UPF), accessed on March 1, 2022.
- [4] A. Dal Corso. Pseudopotentials periodic table: From H to Pu. *Computational Materials Science*, 95:337–350, 2014.
- [5] A. Dal Corso. Pseudopotential copper: Cu.pbe-dn-rrkjus-psl.1.0.0.upf, 2018. [http://pseudopotentials.quantum-espresso.org/upf\\_files/Cu.pbe-dn-rrkjus-psl.1.0.0.UPF](http://pseudopotentials.quantum-espresso.org/upf_files/Cu.pbe-dn-rrkjus-psl.1.0.0.UPF), accessed on March 1, 2022.
- [6] K. Garrity, J. Bennett, K. Rabe, and D. Vanderbilt. Pseudopotential carbon: c.pbe.v1.2.uspp.f.upf, 2014. [https://www.physics.rutgers.edu/gbrv/c\\_pbe\\_v1.2.uspp.F.UPF](https://www.physics.rutgers.edu/gbrv/c_pbe_v1.2.uspp.F.UPF), accessed on March 1, 2022.
- [7] K. Garrity, J. Bennett, K. Rabe, and D. Vanderbilt. Pseudopotential bromine: br.pbe.v1.4.uspp.f.upf, 2015. [https://www.physics.rutgers.edu/gbrv/br\\_pbe\\_v1.4.uspp.F.UPF](https://www.physics.rutgers.edu/gbrv/br_pbe_v1.4.uspp.F.UPF), accessed on March 1, 2022.
- [8] K. Garrity, J. Bennett, K. Rabe, and D. Vanderbilt. Pseudopotential chlorine: cl.pbe.v1.4.uspp.f.upf, 2015. [https://www.physics.rutgers.edu/gbrv/cl\\_pbe\\_v1.4.uspp.F.UPF](https://www.physics.rutgers.edu/gbrv/cl_pbe_v1.4.uspp.F.UPF), accessed on March 1, 2022.
- [9] K. Garrity, J. Bennett, K. Rabe, and D. Vanderbilt. Pseudopotential sulfur: s.pbe.v1.4.uspp.f.upf, 2015. [https://www.physics.rutgers.edu/gbrv/s\\_pbe\\_v1.4.uspp.F.UPF](https://www.physics.rutgers.edu/gbrv/s_pbe_v1.4.uspp.F.UPF), accessed on March 1, 2022.
- [10] K. F. Garrity, J. W. Bennett, K. M. Rabe, and D. Vanderbilt. Pseudopotentials for high-throughput dft calculations. *Computational Materials Science*, 81:446–452, 2014.

- [11] P. Giannozzi, O. Andreussi, T. Brumme, O. Bunau, M. B. Nardelli, M. Calandra, R. Car, C. Cavazzoni, D. Ceresoli, M. Cococcioni, N. Colonna, I. Carnimeo, A. D. Corso, S. de Gironcoli, P. Delugas, R. A. DiStasio, A. Ferretti, A. Floris, G. Fratesi, G. Fugallo, R. Gebauer, U. Gerstmann, F. Giustino, T. Gorni, J. Jia, M. Kawamura, H.-Y. Ko, A. Kokalj, E. Küçükbenli, M. Lazzeri, M. Marsili, N. Marzari, F. Mauri, N. L. Nguyen, H.-V. Nguyen, A. O. de-la Roza, L. Paulatto, S. Poncé, D. Rocca, R. Sabatini, B. Santra, M. Schlipf, A. P. Seitsonen, A. Smogunov, I. Timrov, T. Thonhauser, P. Umari, N. Vast, X. Wu, and S. Baroni. Advanced capabilities for materials modelling with Quantum ESPRESSO. *Journal of Physics: Condensed Matter*, 29(46):465901, 2017.
- [12] P. Giannozzi, S. Baroni, N. Bonini, M. Calandra, R. Car, C. Cavazzoni, D. Ceresoli, G. L. Chiarotti, M. Cococcioni, I. Dabo, A. Dal Corso, S. de Gironcoli, S. Fabris, G. Fratesi, R. Gebauer, U. Gerstmann, C. Gougoussis, A. Kokalj, M. Lazzeri, L. Martin-Samos, N. Marzari, F. Mauri, R. Mazzarello, S. Paolini, A. Pasquarello, L. Paulatto, C. Sbraccia, S. Scandolo, G. Sclauzero, A. P. Seitsonen, A. Smogunov, P. Umari, and R. M. Wentzcovitch. Quantum espresso: a modular and open-source software project for quantum simulations of materials. *Journal of Physics-Condensed Matter*, 21(39):395502, 2009.
- [13] G. Henkelman, B. P. Uberuaga, and H. Jónsson. A climbing image nudged elastic band method for finding saddle points and minimum energy paths. *The Journal of Chemical Physics*, 113(22):9901–9904, 2000.
- [14] S. Kenny, J. Pethica, and R. Edgell. A density functional study of Br on Cu(100) at low coverages. *Surface Science*, 524(1):141–147, 2003.
- [15] G. Kresse and J. Furthmüller. Efficient iterative schemes for ab initio total-energy calculations using a plane-wave basis set. *Phys. Rev. B*, 54:11169–11186, 1996.
- [16] G. Kresse and J. Hafner. Ab initio molecular dynamics for liquid metals. *Phys. Rev. B*, 47:558–561, 1993.
- [17] G. Kresse and J. Hafner. Ab initio molecular-dynamics simulation of the liquid-metal–amorphous-semiconductor transition in germanium. *Phys. Rev. B*, 49:14251–14269, 1994.
- [18] G. Kresse and D. Joubert. From ultrasoft pseudopotentials to the projector augmented-wave method. *Phys. Rev. B*, 59:1758–1775, 1999.
- [19] G. Mills, H. Jónsson, and G. K. Schenter. Reversible work transition state theory: application to dissociative adsorption of hydrogen. *Surface Science*, 324(2):305–337, 1995.

- [20] H. J. Monkhorst and J. D. Pack. Special points for brillouin-zone integrations. *Phys. Rev. B*, 13:5188–5192, 1976.
- [21] J. P. Perdew, K. Burke, and M. Ernzerhof. Generalized gradient approximation made simple. *Phys. Rev. Lett.*, 77:3865–3868, 1996.
- [22] J. P. Perdew and Y. Wang. Accurate and simple analytic representation of the electron-gas correlation energy. *Phys. Rev. B*, 45:13244–13249, 1992.
- [23] Quantum Espresso Foundation. Original QE PP library, 2008. [http://pseudopotentials.quantum-espresso.org/legacy\\_tables/original-qe-pp-library](http://pseudopotentials.quantum-espresso.org/legacy_tables/original-qe-pp-library), accessed on March 1, 2022.
- [24] B. Rahn, R. Wen, L. Deuchler, J. Stremme, A. Franke, E. Pehlke, and O. M. Magnussen. Coadsorbate-induced reversal of solid–liquid interface dynamics. *Angewandte Chemie International Edition*, 57(21):6065–6068, 2018.
- [25] B. Rahn, R. Wen, L. Deuchler, J. Stremme, A. Franke, E. Pehlke, and O. M. Magnussen. Supporting information: Coadsorbate-induced reversal of solid–liquid interface dynamics. *Angewandte Chemie International Edition*, 57(21):6065–6068, 2018.
- [26] D. Sheppard, R. Terrell, and G. Henkelman. Optimization methods for finding minimum energy paths. *The Journal of Chemical Physics*, 128(13):134106, 2008.